Extreme P-, Bi-, Nb-, Sc-, U- and F-rich zircon from fractionated perphosphorous granites: The peraluminous Podlesí granite system, Czech Republic

Karel Breiter [a],*, Hans-Jürgen Förster [b], Radek Škoda [c]

[a] Czech Geological Survey, Geologická 6, CZ-15200 Praha 5, Czech Republic
[b] Institute of Earth Sciences, University of Potsdam, P.O. Box 601553, D-14415 Potsdam, Germany
[c] Institute of Earth Sciences, Masaryk University, Kotlářská 2, CZ-61137 Brno, Czech Republic

Abstract

The strongly peraluminous and P-rich, protolithionite and zinnwaldite leucogranites from Podlesí, western Krušné Hory Mts., Czech Republic, contain accessory zircon with extraordinary enrichment of several elements, which constitute trace elements in common zircon. Elements showing a not yet reported anomalous enrichment include P (up to 20.2 wt.% P_2O_5; equivalent to 0.60 apfu, formula calculated on the basis of 4 oxygen atoms), Bi (up to 9.0 wt.% Bi_2O_3; 0.086 apfu), Nb (up to 6.7 wt.% Nb_2O_5, 0.12 apfu), Sc (up to 3.45 wt.% Sc_2O_3; 0.10 apfu), U (up to 14.8 wt.% UO_2; 0.12 apfu) and F (up to 3.81 wt.% F; 0.42 apfu). Strong enrichment of P preferentially involved the berlinite-type substitution ($2\,Si^{4+} \Leftrightarrow P^{5+} + Al^{3+}$) implying that significant Al may enter the Si position in zircon. Incorporation of other exotic elements is primarily governed by the xenotime ($Si^{4+} + Zr^{4+} \Leftrightarrow P^{5+} + Y^{3+}$), pretulite ($Sc^{3+} + P^{5+} \Leftrightarrow Zr^{4+} + Si^{4+}$), brabantite-type ($Ca^{2+} + (U, Th)^{4+} + 2P^{5+} \Leftrightarrow 2Zr^{4+} + 2Si^{4+}$), and ximengite-type ($Bi^{3+} + P^{5+} \Leftrightarrow Zr^{4+} + Si^{4+}$) substitution reactions. One part of the anomalous zircons formed late-magmatically, from a strongly peraluminous, P–F–U-rich hydrous residual melt that gave rise to the zinnwaldite granite. Interaction with aggressive residual fluids and metamictization have further aided in element enrichment or depletion, particularly in altered parts of zircon contained in the protolithionite granite. Most of the zircon from F-rich greisens have a composition close to endmember $ZrSiO_4$ and are chemically distinct from zircon in its granite parent. This discrepancy implies that at Podlesí, granitic zircon became unstable and completely dissolved during greisenization. Part of the mobilized elements was reprecipitated in newly grown, hydrothermal zircon.
© 2005 Elsevier B.V. All rights reserved.

Keywords: Zircon; Phosphorus; Niobium; Uranium; Bismuth; Scandium; Fluorine; Solid solution; Peraluminous granites

1. Introduction

Elevated contents of phosphorus in zircon (ideally $ZrSiO_4$) were first noted in the 1930s in zircon from granitic pegmatites (4.23 wt.% P_2O_5, Kimura and Hironaka, 1936; 5.3 wt.% P_2O_5, Hata, 1938). Here, as in the majority of P-bearing zircons reported later, enrichment of phosphorus is accompanied by enrichment of yttrium and heavy rare earth elements (HREE) (e.g., Deer et al., 1997; Hoskin and Schaltegger, 2003, and references therein). The simultaneous enrichment of P and (Y+HREE) expresses that both these elements are usually incorporated in the zircon structure according to the coupled substitution mechanism

* Corresponding author. Tel.: +420 251 085508; fax: +420 251 817390.
  E-mail address: breiter@cgu.cz (K. Breiter).

$P^{5+}+(Y,HREE)^{3+} \Leftrightarrow Si^{4+}+Zr^{4+}$ (xenotime-type substitution). Zircon and xenotime are isostructural (tetragonal). Experimentally, zircon crystals containing up to 12.5 mol% YPO_4 (4.98 wt.% P_2O_5) and 8.2 mol% $DyPO_4$ (3.04 wt.% P_2O_5) were synthesized (Hanchar et al., 2001). However, although natural zircon crystals containing up to 25–32 mol% of the xenotime component have been reported occasionally (Speer, 1982; Bea, 1996), a continuous solid-solution series between endmember zircon and xenotime is unlikely to exist (e.g., Förster, 2006-this volume).

Phosphorus-rich zircon poor in (Y+REE) is less common and preferentially occurs in fractionated, peraluminous, P-rich (0.5–1.0 wt.% P_2O_5) granites and pegmatites. Studies of zircon from various occurrences in the Massif Central (France) revealed up to 3.4 wt.% P_2O_5 in zircon from the Chedeville pegmatite (Raimbault, 1998), and up to 3.8 wt.% P_2O_5 in zircon from the Richemont rhyolite (Raimbault and Burnol, 1998). P_2O_5 concentrations approaching 8 wt.% were measured in an initial study of zircon from the Podlesí granite, Czech Republic (Förster, 2001). The Eibenstock Li-mica granite massif in the western part of the German Erzgebirge hosts altered zircon grains, which contain 9.6 wt.% P_2O_5, but only 2 wt.% Y_2O_3 (H.-J. Förster, unpubl. data). 12.8 wt.% P_2O_5 (0.9 wt.% Y_2O_3) was measured in a zircon from fractionated intrusions of the neighbouring two-mica granite suite of Bergen (H.-J. Förster, unpubl. data). The highest P-content in REE-poor zircon reported to date is 15.31 wt.% P_2O_5, from the Yashan granite, China (Huang et al., 2000).

In the frame of an ongoing systematic study of the P-content in silicate minerals of evolved, P-rich peraluminous granites (feldspars: Frýda and Breiter, 1995; topaz: Breiter and Kronz, 2004; garnet: Breiter et al., 2005b), a detailed investigation of zircon from the late-Variscan, peraluminous multiphase Eibenstock–Nejdek massif, in the western Erzgebirge/Krušné Hory of the Czech Republic, has been undertaken. This study revealed the occurrence of unusual zircon grains, with bizarre compositions with respect to P, Nb, U, Bi, Sc and other elements, in the most highly evolved granite series of this massif, the Podlesí granite/dyke-granite/greisen suite (Breiter et al., 2005a). The composition and origin of these zircons form the subject of this paper. Knowledge of this compositional data not only add important information on the mineralogy of zircon itself, but also shows that zircon may act as an important marker for the evolution of granitic magmas during prograde differentiation and subsequent fluid–rock interaction.

2. Geological background

The late-Variscan Nejdek–Eibenstock granite massif (∼325–320 Ma), in the Saxothuringian zone of the Bohemian Massif, is composed of texturally and geochemically distinct, cogenetic intrusions and related greisens (Breiter et al., 1999; Fig. 1). The earliest intrusions comprise albite–topaz–siderophyllite granites (0.1 wt.% F, 0.2 wt.% P_2O_5), followed by fluorine-enriched (0.5–1.0 wt.% F, 0.2–0.4 wt.% P_2O_5) albite–topaz–lithian siderophyllite granites (biotite granite in Fig. 1). The most highly fractionated residual melts of these magmas gave rise to minor, small intrusions of extremely F-, P-, and Li-rich granites making up the Podlesí stock (Breiter et al., 2005a). The Podlesí granite suite forms a tongue-like intrusion of albite–topaz–protolithionite granite (*stock granite*). The upper contact is rimmed by a marginal pegmatite (*stockscheider*). At a depth of 40–100 m, the stock granite is intercalated with flat dykes of albite–topaz–zinnwaldite granite
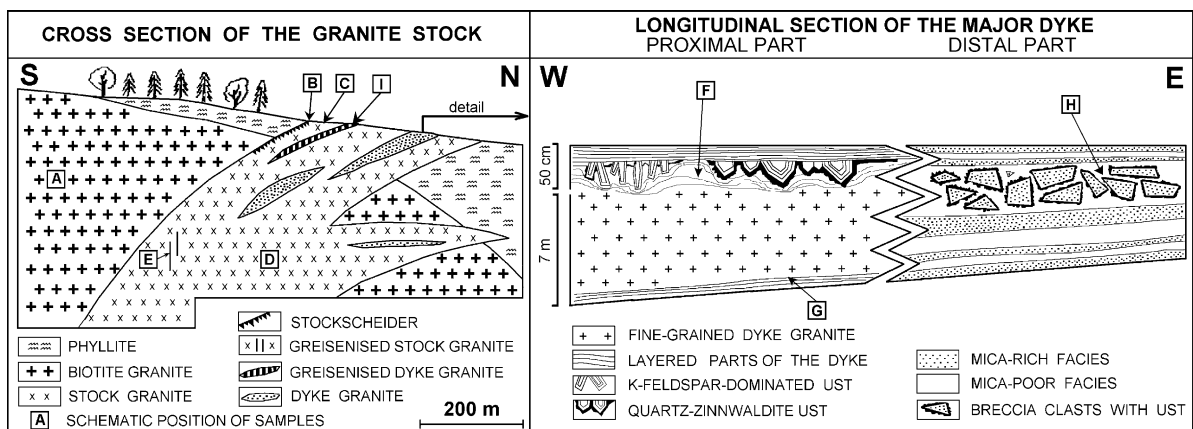

Fig. 1. Simplified geological cross-section of the Podlesí granite stock.

(*dyke granite*). Already the stock granite is strongly fractionated and rich in P (~0.5 wt.% P_2O_5), F (0.5–1.2 wt.%), Ga, Rb, Li, Cs, Sn, Nb, Ta, and W. The dyke granite represents batches of more extremely fractionated residual melts that are even more enriched in P (~1 wt.% P_2O_5), F (1–1.5 wt.%), Rb, Li, Ga, Nb, and Ta. Prominent layering and unidirectional solidification textures (in the sense of Shannon et al., 1982; UST in Fig. 1) proof extreme enrichment of fluxing elements and undercooling of the crystallised melt (London, 1996). The strongest enrichment of lithophile elements is related to the apical parts of the dyke granite, where concentration highs approach 4 wt.% for F, 1 wt.% for Li_2O, and 1.5 wt.% for P_2O_5. These portions of the dykes became late-magmatically *brecciated* and cemented with quartz and albite. Mineralogically (quartz+zinnwaldite+topaz), these domains resemble topazites (Eadington and Nashar, 1978) or rocks synthesised by Xiong et al. (1999) from extremely F-enriched parental melt.

Metasomatic greisens are subordinate. Locally, thin, steep stringers of dark, P–F-rich, but Li-poor greisens composed of quartz, topaz, siderophyllite, and abundant apatite with accessory cassiterite developed in the protolithionite stock granite. One of the dykes of the zinnwaldite granite was transformed into a light, P–F–Li-rich quartz–topaz greisen containing accessory zinnwaldite, wolframite, columbite, phosphates, and various Bi minerals.

3. Analytical methods

240 quantitative electron-microprobe analyses of zircon in 25 representative samples from the Nejdek–Eibenstock granite massif were conducted (Table 1). Zircon was analysed in thin sections, to obtain information about the genetic position of the individual zircon crystal in the rock. Back-scattered electron (BSE) and scanning-electron microscope-cathodoluminescence (SEM-CL) images were performed prior to analysis to study the internal structure of individual zircon crystals. Care was taken that the point analyses were made in areas that appear homogeneous in the back-scattered electron image.

The contents of W, P, Nb, Ta, Si, Zr, Hf, Th, U, Ti, Sn, Al, Sc, Bi, Y, Dy, Er, Yb, Ca, Fe, Mn, Pb, and F in zircon were determined using a CAMECA SX100 electron microprobe (Masaryk University, Brno) equipped with five wavelength-dispersive spectrometers and a CL detector. The accelerating voltage and beam current were 15 kV and 20 or 40 nA, respectively, with beam diameters between 2 and 5

µm. Texturally complicated zircons were measured using a 2-µm spot size and a 20 nA beam current; a 5-µm spot and a 40 nA beam current were used in the analysis of homogenous zircon grains. Complete wavelength-dispersion spectra (WDS) were collected from several zircon crystals to identify the complete spectrum of elements detectable with the electron microprobe. WDS scans of standards and samples and simulated WDS spectra were used to search for overlapping peaks and to accurately determine the background positions. Pulse Height Analyses (PHA) in differential mode was used to eliminate the interference from higher order peaks of other, undesired elements.

The following standards, X-ray lines, and crystals (in parentheses) were used: K_α: Si on augite (TAP), Al on almandine (TAP), P and Ca on apatite (PET), Fe on andradite (LLIF), Mn on rhodonite (LLIF), Ti on TiO (PET), F on topaz (PC1), Sc on ScP_5O_{14} (PET), L_α: Zr on zircon (TAP), Y on YAG (TAP), Yb on YbP_5O_{14} (LLIF), W on metallic W (LLIF), Nb on ferrocolumbite from Ivigtut, Greenland (LPET), Sn on SnO_2 (LPET), L_β: Dy on DyP_5O_{14} (LLIF), Er on YErAG (LLIF), M_α: Th on ThO_2 (LPET), Pb on vanadinite (LPET), Hf on HfO_2 (TAP), Bi on metallic Bi (LPET), Ta on Ta_2O_5 (LPET), and M_β: U on metallic U (LPET). Major elements were measured 20 s on the peak and 10 s for background counts on both sides of the peak. The counting times for minor and trace elements were 40 and 60 s, respectively, and half that time on each background. When only one measured background and a calculated background slope had to be applied, the background counting time was the same as the peak counting time. More sensitive LPET and LLIF crystals were used to determine applicable minor and trace elements. Raw data were converted into concentrations using appropriate PAP matrix corrections (Pouchou and Pichoir, 1985). Typical detection limits and standard deviation are listed in Table 2.

Additional microprobe analyses were conducted using a CAMECA SX50 machine at the Geo-ForschungsZentrum Potsdam operating in the wavelength-dispersion mode. The CAMECA PAP program was used for matrix correction (Pouchou and Pichoir, 1985). The operation conditions involved a 20 kV acceleration voltage, 40 nA beam current, and a beam diameter between 1 and 10 µm. To avoid element diffusion and to minimize decomposition of the altered parts of the grains under the electron bombardment, a maximum possible spot size was chosen. However, because part of the grains are of small size and homogeneous zones were usually narrow, destruction of grains during the 20-min-long analysis could rarely

Table 1
Description of zircon samples

	Rock type	Sample	Description of zircon	Accessory mineral assemblage	WR Zr ppm	WR Zr/Hf atoms	WR Bi ppm	WR U ppm	WR P_2O_5 wt.%
A	Biotite granite	111, 398, 1474, 1633	Early crystals enclosed in mica	Apatite, ilmenite, monazite, topaz	60–80	25–60	1–5	7–28	0.27–0.44
B	Stockscheider	3361	Early crystals enclosed in mica	Topaz, apatite, ilmenite, monazite, wolframite, xenotime	31	31	3	43	0.40
C	Protolithionite granite, upper part of the stock	3359, 3385, 65.7	Mostly late interstitial crystals	Topaz, apatite, ilmenite, monazite, uraninite, wolframite, xenotime, cassiterite	27–37	23–35	1–8	13–44	0.37–0.70
D	Protolithionite granite, lower part of the stock	2686, 2687, 3436, 3443	Mostly late interstitial crystals	Topaz, apatite, ilmenite, monazite, uraninite, xenotime, cassiterite	20–40	36–44	1–4	28–45	0.38–0.50
E	Greisenised protolithionite granite	3365	Both, early and late crystals	Topaz, apatite, ilmenite, cassiterite, wolframite, uraninite, monazite	26	24–35	80–110	14–30	0.48
F	Zinnwaldite granite, upper part of the dyke, laminated rock with UST	3416, 3417, 4011, 4012	Late interstitial crystals	Topaz, amblygonite, columbite, ixiolite, bismuthinite, wolframite, cassiterite	13–34	17–19	8–25, up to 570	28–36	0.8–1.1
G	Zinnwaldite granite, near the lower contact of the dyke	3413, 3663, 3664	Late interstitial crystals	Topaz, ixiolite, fluorite, cassiterite, xenotime, brabantite	18	28	8	13	0.5
H	Zinnwaldite granite, late breccia	3647K, 3647L, 3968	Late interstitial crystals	Topaz, amblygonite, columbite	35	10–14	16–26	7–17	0.57–0.88
I	Greisenised zinnwaldite granite	3389, 3387	Small crystals in quartz and topaz	Topaz, monazite, wolframite, columbite, bismuthinite, native Bi	40	31–35	560–710	29–32	0.33–0.34

Table 2
Standard deviation and detection limits for elements analysed on the CAMECA SX100 machine at the MU Brno

	Standard deviation [wt.%]			Detection limit [ppm]		
	Min	Max	Average	Min	Max	Average
WO_3	0.150	0.211	0.169	1570	2005	1886
P_2O_5	0.033	0.317	0.131	266	355	328
Nb_2O_5	0.066	0.176	0.084	783	939	870
Ta_2O_5	0.097	0.237	0.121	1244	1822	1538
SiO_2	0.091	0.222	0.170	303	572	368
ZrO_2	0.402	0.562	0.511	1018	1222	1162
HfO_2	0.081	0.136	0.109	530	631	582
ThO_2	0.070	0.175	0.079	822	957	880
UO_2	0.085	0.179	0.103	916	1288	989
TiO_2	0.023	0.028	0.024	259	303	284
SnO_2	0.030	0.040	0.033	350	435	391
Al_2O_3	0.013	0.153	0.039	152	188	164
Sc_2O_3	0.019	0.068	0.036	190	220	209
Y_2O_3	0.040	0.088	0.044	459	536	511
Bi_2O_3	0.121	0.283	0.161	1392	1705	1542
Dy_2O_3	0.177	0.205	0.193	2123	2458	2322
Er_2O_3	0.211	0.269	0.249	2585	3413	3094
Yb_2O_3	0.119	0.144	0.132	1388	1664	1577
CaO	0.025	0.113	0.052	268	310	294
FeO	0.038	0.482	0.062	395	523	433
MnO	0.035	0.071	0.043	390	455	424
PbO	0.068	0.095	0.076	818	1030	953
F	0.044	0.163	0.066	531	695	573

been avoided. Counting times, data reduction, analysing crystals, X-ray lines, standards, and line-interference correction procedures are described in detail in Förster (1998).

Particular care was taken to confirm by X-ray mapping or high-resolution BSE imaging that the elements measured are part of the zircon structure and not entrained in accidentally analysed mineral inclusions.

4. Results

Representative results of electron-microprobe analyses of zircon grains from the various types of rocks are listed in Table 3. The Fig. 2 shows BSE and secondary electron (SE) images showing the typical shape and appearance of zircon from Podlesí. The Fig. 3 is a collection of x–y diagrams illustrating the relations between chemically important elements (in apfu) in the analysed zircons. The spatial distribution of selected elements inside of typical zircon grains is displayed in the Fig. 4.

4.1. Petrography

The less fractionated lithian-siderophyllite (biotite) granite contains dominantly early magmatic, oscillato-

ry-zoned zircon crystals (100–150 μm) with moderate CL, hosted in biotite. Compositional zonation of the majority of grains refers to fractional evolution of the parental melt: cores are chemically near to endmember $ZrSiO_4$, rims are enriched in Hf, U, P, and other elements (Fig. 2a, sample 1474). Crystals with a homogeneous, P-, U-poor core and an oscillatory-zoned, U-, P-enriched rim also occur (Fig. 2b, sample 398).

In the protolithionite stock granite, small (<30 μm), late-magmatic, sub- to euhedral crystals predominate over altered, early magmatic zircon hosted in mica. Most late grains are corroded, patchyly zoned, contain abundant vacuoles, and rarely inclusions of uraninite and Nb minerals (Fig. 2c, d). They occur interstitially between quartz, topaz, albite, and apatite. Zircons in the lower part of this granite tend to be xenomorph and more fractured. In the zinnwaldite dyke granite, only small: late interstitial zircon occurs. In size, shape, and degree of alteration, the zircon grains from this rock type principally resemble those from the protolithionite stock granite. The late crystals typically have patchy, metamict cores with crystalline, relatively unaltered rims (Fig. 2e, f). Chemical zonality is only occasionally evolved: expressed with thin rims enriched in Hf and depleted in U and P.

Zircon from the greisenized protolithionite stock granite is of variable size (10–60 μm), sub- to euhedral, and vacuolized. Most grains are included in Li mica or occur interstitially between mica, topaz, and quartz (Fig. 2g). Zircon from the zinnwaldite dyke granite-greisens is usually less than 30 μm in size, sub- to euhedral, vacuolized, and weakly corroded and patchy-zoned (Fig. 2h). It occurs preferentially in quartz and topaz and is partly mantled by bismuthinite.

4.2. Chemical composition

Zircon in all granite types is chemically highly variable, even at the scales of one thin section or individual grain (Table 3). However, a systematic shift in zircon composition between the early biotite granites and the late zinnwaldite dyke granites is obvious. With increasing degree of melt fractionation, zircon composition changes from U-, Hf-, P-poor, well-zoned, unaltered crystals stoichiometrically close to endmember $ZrSiO_4$ to U-, P-, Al-, Ca-, Fe-, F-rich, hydrated, patchy-zoned and strongly altered, metamict grains depleted in Zr and Si.

4.2.1. Phosphorus
The most intriguing feature of the zircon from Podlesí consists in the enrichment of P, which is not

124

Table 3
Representative electron-microprobe analyses and structural formulae of zircon from Podlesí

Rock	A	A	A	B	B	C	C	C	C	C	D	D	D	D	E	E	F	F
Sample	398	398	111	3361	3361	3385	3385	3359	3359	3359	3436	3436	3436	2686	3365	3365	3416	3417
Position	zr3,core	zr3,rim	zr2	zr2/1	zr3/1	zr6/1	zr6/2	zr9/2	zr2/2h	zr4/2	zr1/1	zr10/3	zr9/2	zr1,core	zr1/1	zr 2/1	zr6/2	zr7/1
Anal. no.	1	2	3	4	5	6	7	8	9	10	11	12	13	14	15	16	17	18
P_2O_5	0.17	7.96	12.82	0.17	7.57	7.26	0.25	5.35	6.22	0.00	0.97	5.88	6.02	10.99	0.44	0.03	2.66	12.03
Nb_2O_5	na	na	na	na	na	na	na	**6.29**	**2.57**	0.00	0.00	1.02	1.76	na	na	0.00	0.00	2.35
Ta_2O_5	na	na	na	na	na	na	na	na	na	na	na	na	na	na	na	na	na	na
SiO_2	32.25	19.71	13.54	30.92	22.61	20.03	30.96	18.25	19.49	30.20	30.65	20.48	20.80	*16.25*	30.75	32.49	22.25	14.48
ZrO_2	65.10	49.40	44.76	62.10	39.13	42.85	63.33	*34.19*	40.60	53.97	57.73	41.25	*36.06*	52.41	61.19	62.73	49.67	39.07
HfO_2	1.06	1.70	1.79	3.51	1.94	1.89	3.29	1.38	1.75	**9.09**	4.63	1.96	1.65	2.08	3.77	4.32	2.66	1.68
ThO_2	0.00	0.20	0.47	0.00	0.76	**6.64**	0.06	3.51	1.89	0.01	0.03	0.14	0.59	0.07	0.05	0.00	0.12	0.65
UO_2	0.11	1.82	2.42	0.17	2.13	3.27	0.52	2.86	2.20	1.21	1.87	**8.95**	**14.75**	1.52	0.58	0.26	3.95	3.41
TiO_2	0.00	0.15	0.27	na	na	na	na	0.19	0.04	0.02	0.03	0.10	0.16	0.12	na	0.00	0.00	0.21
Al_2O_3	0.01	1.25	2.05	0.04	2.14	1.70	0.04	0.74	4.10	0.19	0.19	1.09	1.05	2.27	0.15	0.02	2.20	**5.49**
Sc_2O_3	0.02	0.24	0.32	0.18	0.45	0.97	0.34	0.44	1.39	0.24	0.48	0.66	0.52	0.29	0.34	0.09	**3.42**	**1.93**
Y_2O_3	0.12	2.34	1.74	0.00	**7.93**	1.08	0.00	0.49	1.04	0.00	0.00	1.23	0.79	1.02	0.00	0.00	0.00	1.13
Bi_2O_3	0.00	0.16	1.49	na	na	na	na	**7.68**	**6.99**	0.00	0.00	0.00	0.00	0.00	na	0.00	0.00	**5.61**
Ce_2O_3	na	na	na	0.01	0.09	0.09	0.00	0.00	0.00	0.00	0.00	0.13	0.07	na	0.00	0.04	0.05	0.00
Nd_2O_3	na	na	na	0.01	0.13	0.15	0.06	0.00	0.00	0.00	0.00	0.00	0.05	na	0.02	0.02	0.02	0.00
Sm_2O_3	na	na	na	0.00	0.18	0.06	0.02	0.00	0.00	0.00	0.00	0.00	0.06	na	0.09	0.04	0.00	0.00
Gd_2O_3	na	na	na	0.02	1.04	0.21	0.01	0.18	0.05	0.00	0.00	0.11	0.08	na	0.00	0.00	0.06	0.14
Dy_2O_3	0.00	0.21	0.16	0.02	1.41	0.19	0.03	0.03	0.15	0.00	0.04	0.41	0.06	0.34	0.04	0.00	0.00	0.08
Yb_2O_3	0.05	0.28	0.19	0.01	0.52	0.17	0.06	0.07	0.18	0.00	0.05	0.32	0.14	0.19	0.09	0.00	0.03	0.12
CaO	0.00	2.47	2.70	0.01	0.86	1.41	0.04	0.77	0.77	0.38	0.46	**3.01**	2.79	**3.80**	0.20	0.00	1.67	1.57
FeO	0.70	**3.59**	1.00	**3.07**	1.27	1.23	0.14	2.76	2.05	0.80	0.46	0.85	0.44	1.64	1.05	0.00	1.36	0.24
MnO	0.03	0.35	0.27	na	na	na	na	0.05	0.06	0.18	0.17	0.69	0.65	0.30	na	0.00	0.30	0.21
PbO	0.00	0.01	0.07	0.07	0.00	0.08	0.08	0.17	0.16	0.13	0.00	0.00	0.00	0.00	0.04	0.00	0.10	0.06
F	0.00	1.77	1.96	0.00	0.80	0.51	0.00	0.47	1.69	0.79	0.00	0.78	0.54	1.86	0.00	0.00	0.59	0.60
$F=O_2$	0.00	0.75	0.83	0.00	0.34	0.22	0.00	0.20	0.71	0.33	0.00	0.33	0.23	0.79	0.00	0.00	0.25	0.25
Total	99.60	93.59	88.00	100.29	90.62	89.56	99.23	88.77	92.67	96.87	97.74	88.74	88.79	95.14	98.80	100.03	90.84	90.78
P	0.004	0.230	0.392	0.005	0.221	0.222	0.007	0.180	0.187	0.000	0.026	0.183	0.191	0.310	0.012	0.001	0.079	0.352
Nb								0.113	0.041	0.000	0.000	0.017	0.030			0.000	0.000	0.037
Ta																		
Si	0.994	0.673	0.489	0.968	0.779	0.723	0.974	0.724	0.690	1.001	0.979	0.752	0.779	0.541	0.973	1.007	0.784	0.500
Zr	0.979	0.822	0.789	0.948	0.657	0.754	0.972	0.661	0.701	0.872	0.899	0.739	0.659	0.851	0.944	0.949	0.853	0.658
Hf	0.009	0.017	0.018	0.031	0.019	0.019	0.030	0.016	0.018	0.086	0.042	0.021	0.018	0.020	0.034	0.038	0.027	0.017
Th	0.000	0.002	0.004	0.000	0.006	0.055	0.000	0.032	0.015	0.000	0.000	0.001	0.005	0.001	0.000	0.000	0.001	0.005
U	0.001	0.014	0.019	0.001	0.016	0.026	0.004	0.025	0.017	0.009	0.013	0.073	0.123	0.011	0.004	0.002	0.031	0.026
Ti	0.000	0.004	0.007					0.006	0.001	0.000	0.001	0.003	0.005	0.003	0.000	0.000	0.000	0.005
Al	0.000	0.050	0.087	0.001	0.087	0.072	0.002	0.035	0.171	0.007	0.007	0.047	0.046	0.089	0.006	0.001	0.091	0.223
Sc	0.001	0.007	0.010	0.005	0.013	0.030	0.009	0.015	0.043	0.007	0.013	0.021	0.017	0.008	0.009	0.002	0.105	0.058
Y	0.002	0.042	0.034	0.000	0.145	0.021	0.000	0.010	0.020	0.000	0.000	0.024	0.016	0.018	0.000	0.000	0.000	0.021
Bi	0.000	0.001	0.014					0.079	0.064	0.000	0.000	0.000	0.000	0.000			0.000	0.050
Ce				0.000	0.001	0.001	0.000	0.000	0.000	0.000	0.000	0.002	0.001		0.000	0.000	0.001	0.000
Nd				0.000	0.002	0.002	0.001	0.000	0.000	0.000	0.000	0.000	0.001		0.000	0.000	0.000	0.000
Sm				0.000	0.002	0.001	0.000	0.000	0.000	0.000	0.000	0.000	0.001		0.001	0.000	0.000	0.000
Gd				0.000	0.012	0.002	0.000	0.002	0.001	0.000	0.000	0.001	0.001		0.000	0.000	0.001	0.002
Dy	0.000	0.002	0.002	0.000	0.016	0.002	0.000	0.000	0.002	0.000	0.000	0.005	0.001	0.004	0.000	0.000	0.000	0.001
Yb	0.000	0.003	0.002	0.000	0.005	0.002	0.001	0.001	0.002	0.000	0.000	0.004	0.002	0.002	0.001	0.000	0.000	0.001
Ca	0.000	0.090	0.104	0.000	0.032	0.054	0.001	0.033	0.029	0.013	0.016	0.118	0.112	0.136	0.007	0.000	0.063	0.058
Fe	0.018	0.103	0.030	0.080	0.036	0.037	0.004	0.092	0.061	0.022	0.012	0.026	0.014	0.046	0.028	0.000	0.040	0.007
Mn	0.001	0.010	0.008					0.002	0.002	0.005	0.005	0.022	0.021	0.008		0.000	0.009	0.006
Pb	0.000	0.000	0.001	0.001	0.000	0.001	0.001	0.002	0.002	0.001	0.000	0.000	0.000	0.000	0.000	0.000	0.001	0.001
F	0.000	0.185	0.224	0.000	0.085	0.058	0.000	0.056	0.189	0.083	0.000	0.090	0.064	0.192	0.000	0.000	0.066	0.066

Structural formula calculated on the basis of 4 oxygen atoms. For explanation of the rock type see Table 1. na=not analyzed. 0.00=below detection limit. Extremely high values are marked in bold, extremely low values in italics.

| G	G	G	G	H	H	H	H	H	H	H	H	H	H	H	H	I	I	I
3664b	3664b	3664	3413	3747/L	3747/L	3747/L	3747/L	3747/L	3747/L	3747L	3747K	3747K	3747K	3968A	3968A	3389	3389	3387
core	rim	41	zr2/1	zr3,core	zr3,rim	93/1	94/1	zr2	zr2	5 / 1 .	zr2,core	zr2,rim	zr2	24 / 1 .	30 / 1 .	zr1/1	zr1/2	19 / 1 .
19	20	21	22	23	24	25	26	27	28	29	30	31	32	33	34	35	36	37
5.67	2.85	11.70	7.25	**20.22**	1.67	**19.12**	4.17	0.72	**15.23**	18.97	6.39	1.60	6.64	17.96	19.87	0.15	0.00	10.21
na	na	na	0.29	na	na	na	na	na	na	1.60	na	na	na	**2.02**	1.78	0.00	0.00	0.00
na	na	na	na	na	na	na	na	na	na	0.04	na	na	na	0.08	**0.35**	na	na	0.00
22.31	27.84	14.65	19.77	*8.16*	29.96	*12.95*	27.66	31.16	*14.81*	9.11	18.69	30.18	18.95	*9.27*	*12.36*	31.82	32.25	14.58
53.58	56.35	47.27	50.96	40.64	59.87	42.37	56.19	60.90	47.16	41.30	48.14	58.42	50.66	37.03	31.96	64.27	63.18	46.37
4.25	4.64	2.15	2.48	2.87	6.73	3.15	**7.81**	5.97	4.08	3.18	4.61	5.37	5.53	2.01	2.82	3.00	3.55	2.28
0.05	0.07	0.11	0.12	0.03	0.00	0.15	0.01	0.00	0.07	0.05	0.01	0.01	0.02	0.17	0.06	0.02	0.04	0.04
0.93	0.86	2.02	2.27	1.29	0.20	1.25	0.37	0.17	0.80	1.84	3.58	0.54	3.11	1.50	0.68	0.39	0.68	2.89
0.14	0.07	0.07	0.02	0.16	0.02	0.18	0.04	0.00	0.15	0.17	0.01	0.03	0.01	0.14	0.41	na	0.00	0.09
1.23	0.62	2.49	1.55	3.30	0.31	3.47	0.72	0.12	2.99	3.42	1.57	0.45	1.82	4.35	1.14	0.01	0.00	1.78
0.29	0.37	0.62	2.11	0.57	0.36	0.80	0.57	0.28	0.36	0.82	1.14	0.86	0.79	0.63	0.36	0.11	0.47	0.55
0.43	0.30	0.90	0.03	0.28	0.00	0.22	0.00	0.00	0.00	0.32	0.00	0.00	0.00	0.29	0.00	0.06	0.00	0.98
2.54	0.97	**5.88**	0.00	2.45	0.00	na	na	0.00	0.00	2.48	0.00	0.00	0.00	1.63	0.02	na	0.00	**9.01**
na	na	na	0.05	na	na	0.02	0.00	na	na	na	na	na	na	na	na	0.00	0.00	na
na	na	na	0.07	na	na	0.05	0.00	na	na	na	na	na	na	na	na	0.00	0.00	na
na	na	na	0.03	na	na	0.00	0.03	na	na	na	na	na	na	na	na	0.03	0.00	na
na	na	na	0.00	na	na	na	na	na	na	na	na	na	na	na	na	0.03	0.00	na
0.24	0.06	0.00	0.04	0.00	0.00	0.18	0.01	0.00	0.00	0.00	0.00	0.00	0.00	0.00	0.00	0.04	0.00	0.14
0.08	0.14	0.28	0.05	0.14	0.16	0.06	0.00	0.00	0.00	0.01	0.00	0.00	0.00	0.07	0.00	0.06	0.00	0.28
0.91	0.41	1.52	2.68	3.71	0.25	3.12	0.49	0.07	1.98	3.70	1.25	0.09	1.05	4.48	3.49	0.00	0.00	0.44
1.48	1.87	0.84	1.74	1.00	0.05	2.06	0.24	0.01	0.55	1.48	0.70	0.50	1.43	0.24	1.08	0.00	0.00	0.91
0.10	0.04	0.21	0.64	0.69	0.05	0.00	0.00	0.01	0.30	0.64	1.02	0.09	1.41	0.60	0.37	na	0.00	0.14
0.00	0.00	0.00	0.00	0.04	0.00	0.05	0.00	0.00	0.03	0.03	0.00	0.01	0.00	0.00	0.00	0.02	0.01	0.00
0.53	0.21	1.27	3.54	1.57	0.00	0.00	0.00	0.00	0.85	0.79	2.42	0.16	2.35	2.13	1.08	0.00	0.00	0.48
0.23	0.09	0.54	1.49	0.66	0.00	0.00	0.00	0.00	0.36	0.33	1.03	0.07	1.00	0.90	0.45	0.00	0.00	0.20
94.74	97.67	92.18	94.19	87.09	99.72	89.27	98.45	99.49	89.48	89.95	89.54	98.38	93.83	84.63	77.83	100.00	100.18	91.17
0.162	0.078	0.350	0.208	0.598	0.044	0.527	0.112	0.019	0.432	0.547	0.198	0.043	0.198	0.543	0.611	0.004	0.000	0.319
			0.004							0.025				0.033	0.029	0.000	0.000	
														0.001	0.003			
0.754	0.897	0.517	0.671	0.285	0.942	0.421	0.875	0.978	0.496	0.310	0.685	0.954	0.667	0.331	0.449	0.988	0.999	0.538
0.884	0.885	0.814	0.843	0.693	0.918	0.672	0.867	0.932	0.771	0.686	0.860	0.900	0.869	0.645	0.566	0.973	0.955	0.834
0.041	0.043	0.022	0.024	0.029	0.060	0.029	0.071	0.054	0.039	0.031	0.048	0.048	0.056	0.021	0.029	0.027	0.031	0.024
0.000	0.001	0.001	0.001	0.000	0.000	0.001	0.000	0.000	0.001	0.000	0.000	0.000	0.000	0.001	0.001	0.000	0.000	0.000
0.007	0.006	0.016	0.017	0.010	0.001	0.009	0.003	0.001	0.006	0.014	0.029	0.004	0.024	0.012	0.005	0.003	0.005	0.024
0.004	0.002	0.002	0.001	0.004	0.000	0.004	0.001	0.000	0.004	0.004	0.000	0.001	0.000	0.004	0.011		0.000	0.003
0.049	0.023	0.104	0.062	0.136	0.011	0.133	0.027	0.004	0.118	0.137	0.068	0.017	0.076	0.183	0.049	0.001	0.000	0.077
0.008	0.010	0.019	0.062	0.017	0.010	0.023	0.016	0.008	0.010	0.024	0.037	0.024	0.024	0.020	0.011	0.003	0.013	0.018
0.008	0.005	0.017	0.001	0.005	0.000	0.004	0.000	0.000	0.000	0.006	0.000	0.000	0.000	0.006	0.000	0.001	0.000	0.019
0.022	0.008	0.054	0.000	0.022	0.000			0.000	0.000	0.022	0.000	0.000	0.000	0.015	0.000		0.000	0.086
			0.001			0.000	0.000			0.000				0.000	0.000	0.000	0.000	0.000
			0.001			0.001	0.000			0.000				0.000	0.000	0.000	0.000	0.000
			0.000			0.000	0.000									0.000	0.000	
			0.000													0.000	0.000	
0.003	0.001	0.000	0.000	0.000	0.000	0.002	0.000	0.000	0.000	0.000	0.000	0.000	0.000	0.000	0.000	0.000	0.000	0.002
0.001	0.001	0.003	0.001	0.001	0.002	0.001	0.000	0.000	0.000	0.000	0.000	0.000	0.000	0.001	0.000	0.001	0.000	0.003
0.033	0.014	0.057	0.097	0.139	0.009	0.109	0.017	0.002	0.071	0.135	0.049	0.003	0.040	0.171	0.136	0.000	0.000	0.017
0.042	0.050	0.025	0.049	0.029	0.001	0.056	0.006	0.000	0.015	0.042	0.021	0.013	0.042	0.007	0.033	0.000	0.000	0.028
0.003	0.001	0.006	0.018	0.021	0.001			0.000	0.008	0.018	0.032	0.003	0.042	0.018	0.011		0.000	0.004
0.000	0.000	0.000	0.000	0.000	0.000	0.000	0.000	0.000	0.000	0.000	0.000	0.000	0.000	0.000	0.000	0.000	0.000	0.000
0.056	0.021	0.141	0.379	0.175	0.000	0.000	0.000	0.000	0.090	0.092	0.280	0.016	0.261	0.240	0.124	0.000	0.000	0.055
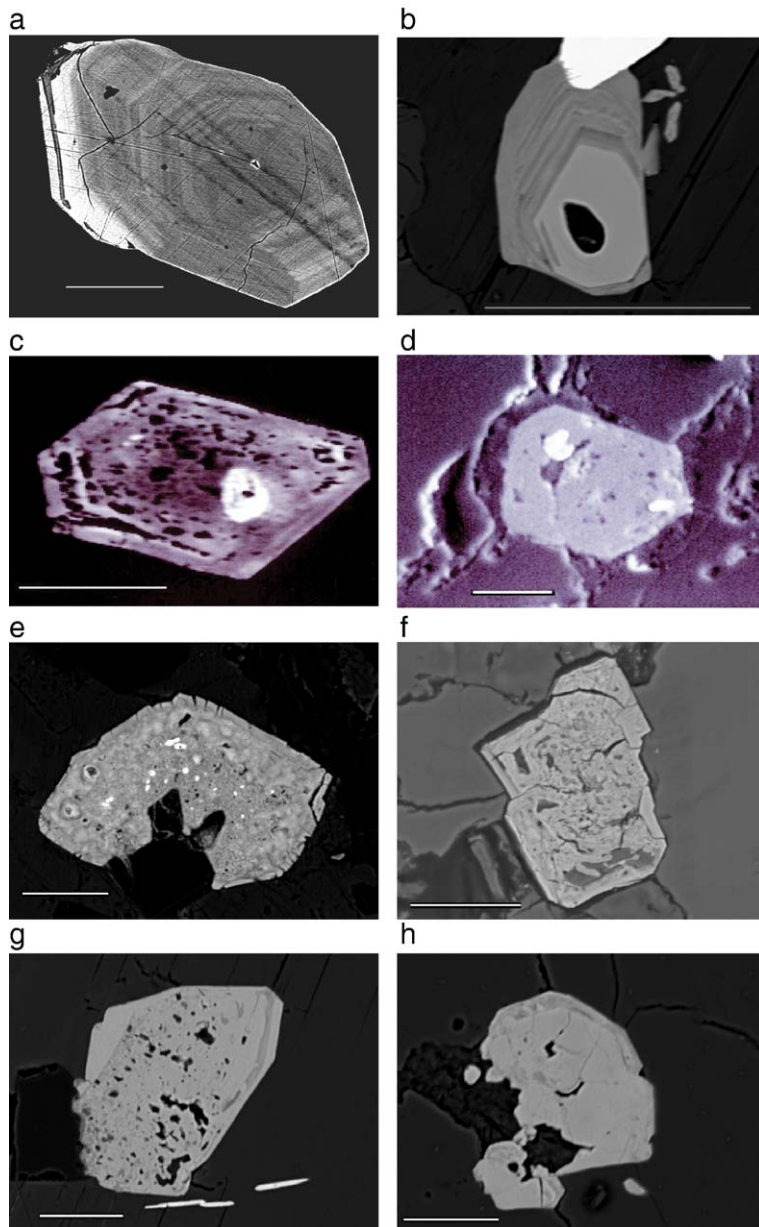
Fig. 2. BSE and SE images of typical zircon grains. Scale bars: 50 µm in Fig. a and b; 20 µm in all other figures. a. BSE image of an euhedral, early magmatic zircon included in biotite (sample 1474, biotite granite). The grain is oscillatory zoned, with the bright rim enriched in uranium. b. BSE image of a subhedral, early magmatic zircon included in biotite (sample 398, biotite granite, compare Table 3, anal. 1 and 2). The grain has a homogeneous core and an oscillatory-zoned rim. The dark grain in the zircon core is an inclusion of quartz, the bright mineral is monazite. c. BSE image of an euhedral, patchy-zoned and vacuolized zircon rich in P, U, and Ca (compare Table 3, anal. 12) included in mica (sample 3436, lower part of the stock granite). Bright areas reflect higher contents of U. The roundish bright area in the interior of the grain marks the position of an electron spot with a 10-µm beam size. d. SE image of a zircon grain reflecting the typical appearance of zircon from the stock granite (sample 3436). The surrounding mineral is topaz. Bright grains inside of the zircon are uraninite inclusions. e. BSE image of a late interstitial zircon associated with zinnwaldite and topaz (sample 3747K, fragment from the brecciated dyke granite, compare Table 3, anal. 30–32). f. BSE image of a late interstitial zircon associated with zinnwaldite and topaz (sample 3747L, matrix of the brecciated dyke granite, compare Table 3, anal. 23 and 24). g. BSE image of a zircon associated with lithian biotite and topaz in the greisenised stock granite (sample 3365). h. BSE image of an interstitial zircon enclosed in quartz from the greisenised dyke granite (sample 3387). The core represents pure zircon, the rim is extremely enriched in bismuth (compare Table 3, anal. 37).

associated with a simultaneous enrichment of (Y + REE). Remarkable P contents were already measured in a small number of zircon grains from the biotite granite (12.8 wt.% P_2O_5, equivalent to 0.39 P atoms-per-formula-unit, *apfu*, formulae calculated on the basis of 4 oxygen atoms; cf. Table 3, anal. 3). In the late zircon from the highest fractionated zinnwaldite dyke granite, the P content approaches 20.22 wt.% of P_2O_5 (0.60 apfu P; Table 3, anal. 23). A high concentration of P is typically accompanied by elevated to strong enrichment of U, Al, Ca, and Fe

(Fig. 4). In each sample, all these elements are positively correlated with P, but substantial differences in Me:P-ratio exist between individual samples from the same rock and, of course, between the different rock types (Fig. 5).

4.2.2. Uranium

Enrichment of uranium is another compositional feature characteristic for zircon from this locality. Distribution of U in individual grains is extremely irregular and no systematic core-to-rim evolution is observed.
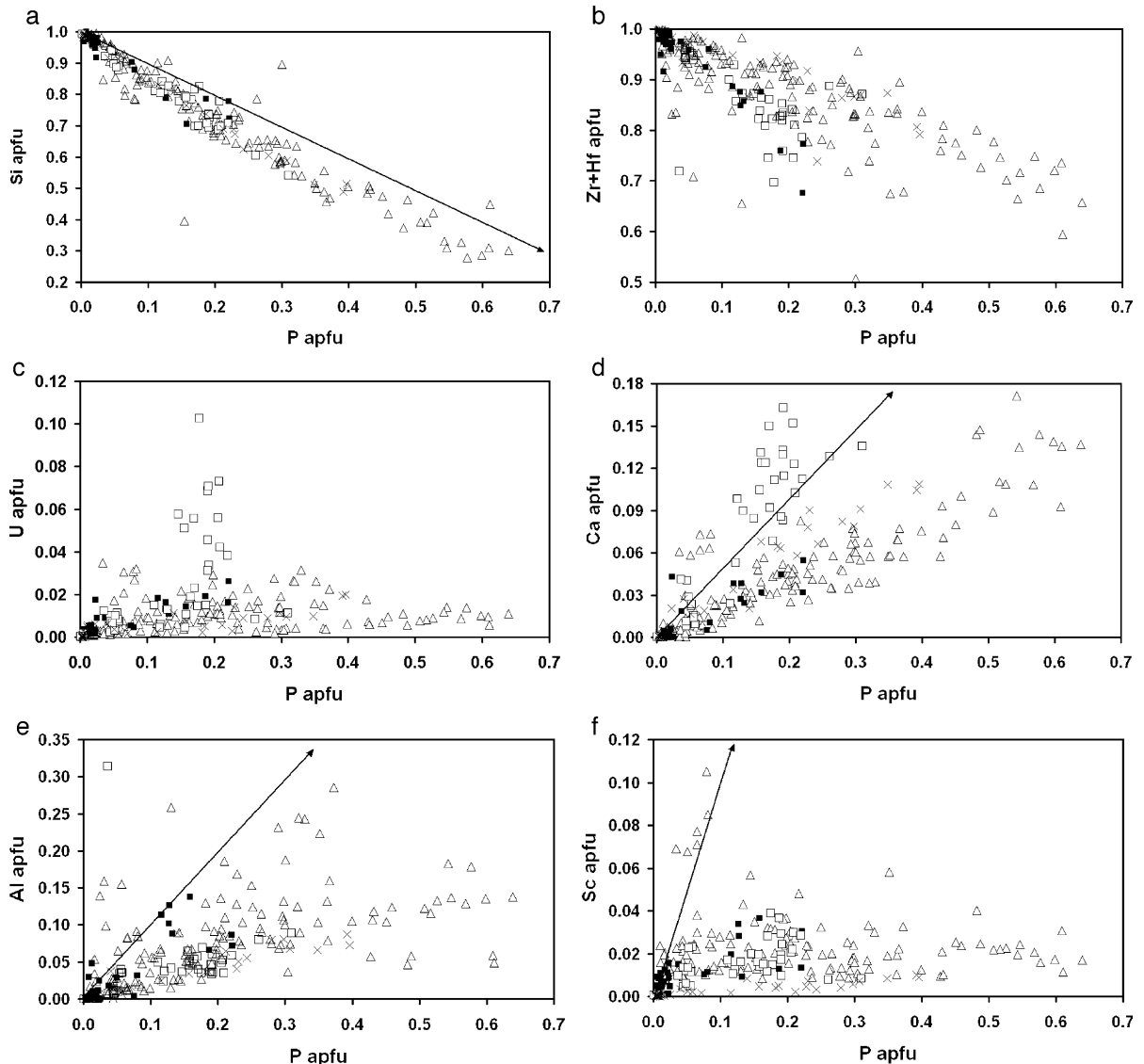
Fig. 3. Plots of P versus Si, (Zr+Hf), U, Ca, Al, Sc, Bi, Y, (Nb+Ta), (Zr/Hf), and F in zircon (in apfu). Symbols: x—zircon from the biotite granite, filled squares—zircon from the upper stock granite, open squares—zircon from the deeper stock granite, triangles—zircon from the dyke granite. The arrows represent vectors of the ideal Si ⇔ P substitution, brabantite-type (P:Ca=2:1), berlinite-type (P:Al=1:1), pretulite (P:Sc=1:1), ximengite-type (P:Bi=1:1) and xenotime (P:(Y+REE)=1:1) substitutions.
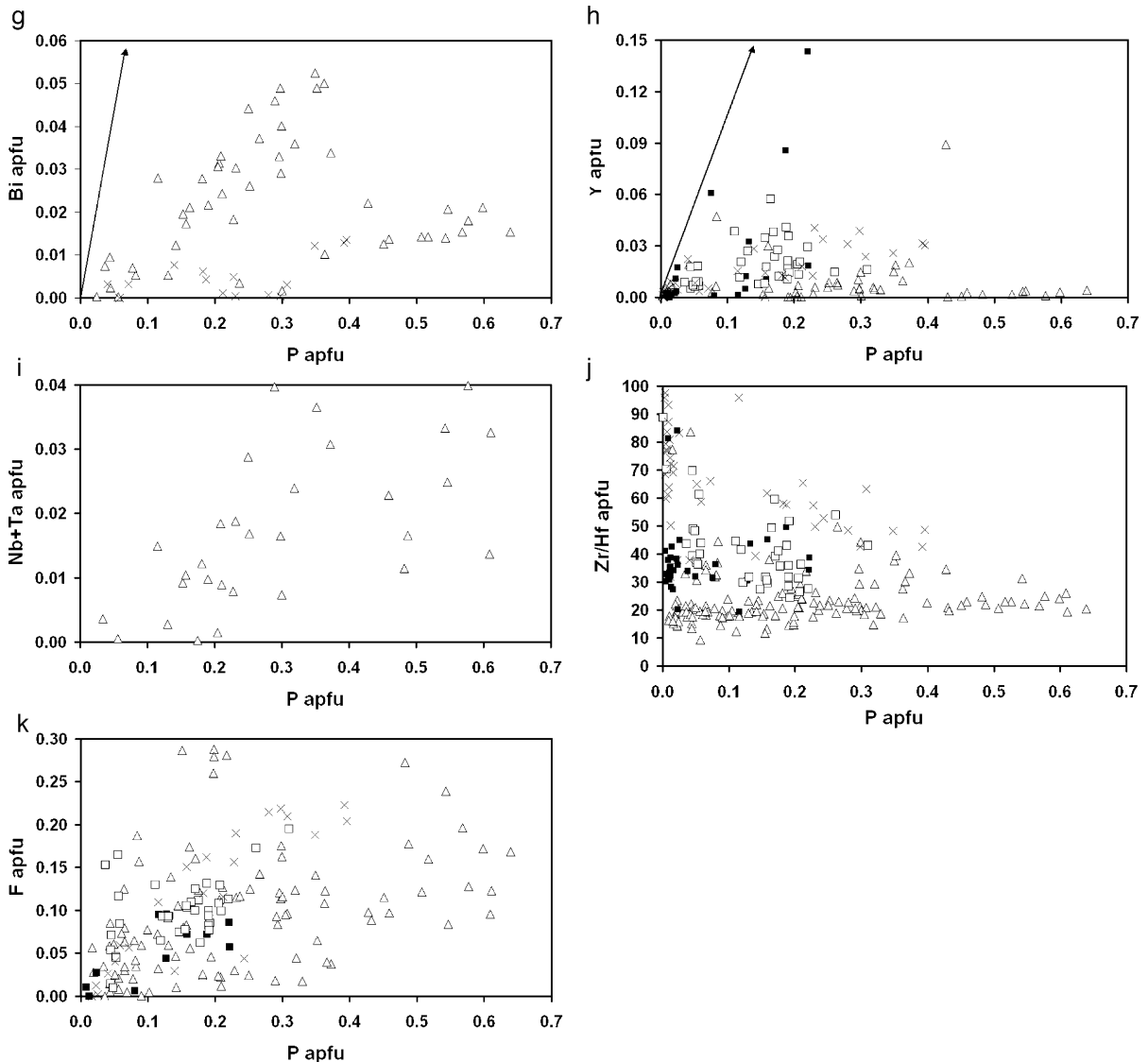
Fig. 3 (continued).

Zircon grains with more than 1 wt.% UO_2 are metamict and hydrated (analytical totals < 98 wt.%). The degree of U enrichment in zircon is independent of the granite type: up to 2.4 wt.% UO_2 in the biotite granite, up to 14.75 wt.% UO_2 in the protolithionite stock granite (Table 3, anal. 13), and up to 6.2 wt.% UO_2 in the zinnwaldite dyke granite.

4.2.3. Bismuth

The concentration of Bi in zircon from Podlesí is heterogeneous at every scale of observation. Zircons enriched in Bi occur together with zircons containing Bi below the microprobe detection limit. Although Bi is not universally correlated with any other element in the zircon, it tends to be enriched in those portions of the zircon grains that contain elevated abundances of P, Al, Ca, Fe, and Mn and are depleted in Si, Zr, and Hf. Strong enrichment of Bi in a granitic zircon relates to bright areas in zoned zircon grains from sample 3359 representing the upper part of the protolithionite stock granite (7.7 wt.% Bi_2O_3, equivalent to 0.079 apfu Bi; Table 3, anal. 8). Bismuth enrichment, however, is not confined to this type of rock, but also is observed in a selection of zircons from the least-fractionated biotite

129
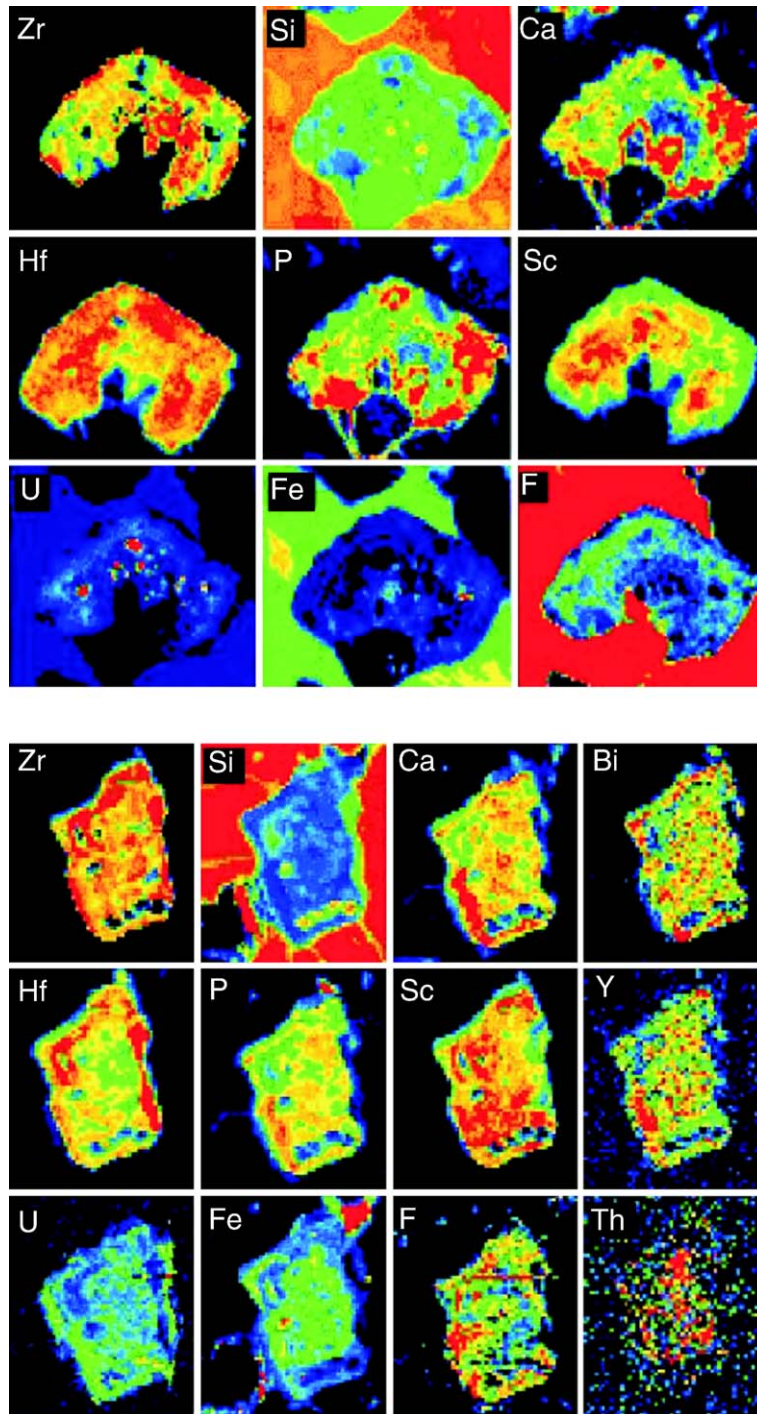
Fig. 4. False-colour X-ray elemental distribution maps for two zircon grains from the brecciated dyke granite. a: Sample 3747K-zircon from the breccia fragment; b: sample 3747L- zircon from the breccia matrix. See Fig. 2e and f for BSE image and size of the grain. The lowest concentrations of an element are shown by cold colours (blue–violet), whilst the highest accumulations are shown in warm colours (red–orange).

granite (1.5 wt.% Bi_2O_3), the zinnwaldite dyke granite (5.9 wt.% Bi_2O_3), and the brecciated zinnwaldite dyke granite (2.5 wt.% Bi_2O_3). The highest Bi concentration (9 wt.% Bi_2O_3; 0.086 apfu Bi) was measured in a zircon from the greisenized zinnwaldite granite (sample 3387; Table 3, anal. 37).

130
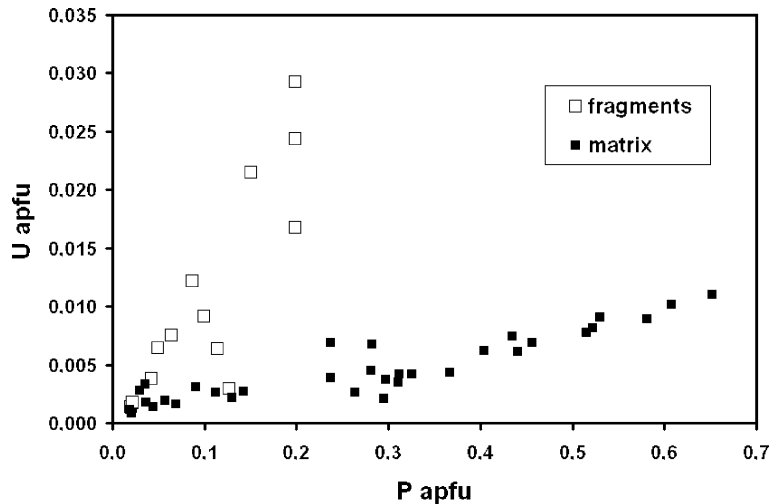
Fig. 5. Plot of P versus U (in apfu) in zircon from the brecciated dyke granite. The different P/U-ratios should fingerprint the parental media (evolved melt, fluid) from which the zircons crystallised.

4.2.4. Scandium

Relative to P, U, and Bi, the concentration of Sc in zircon is less variable and normally range from below the detection limit to 1.5 wt.% Sc_2O_3. In one zircon grain from sample 3416 from the upper part of the zinnwaldite dyke granite, Sc_2O_3 concentrations between 2.33 and 3.42 wt.% (0.11 apfu Sc) were measured (Table 3, anal. 17).

4.2.5. Niobium and tantalum

The concentration of Nb in zircon is heterogeneous and displays no correlation with the rock type. In the protolithionite stock as well as in the zinnwaldite dyke granite, zircon may contain up to 2 wt.% Nb_2O_5. One grain in sample 3359 (upper part of the protolithionite stock granite) contained between 6.3 (Table 3, anal. 8) and 6.7 wt.% Nb_2O_5 (0.12 apfu Nb). Ta was measured only in a small selection of zircon grains, where its concentration was commonly less than 0.1 wt.% Ta_2O_5.

4.2.6. Fluorine

Fluorine is present usually in those zircon grains, which are distinguished by low analytical totals. It tends to be enriched in those grains that are also enriched in U, i.e., are metamict. Fluorine reaches up to 1.8 wt.% in zircon from the biotite granite and protolithionite stock granites, and up to 3.5 wt.% in zircon from the zinnwaldite dyke granite (Table 3, anal. 22). In greisens, the majority of zircon contains no detectable F. Fluorine correlates well with phosphorus in zircon from the biotite granite, but no correlations occur in zircon from the other lithologies.

4.2.7. Other elements

Aluminium is positively correlated with P (Fig. 3). Zircon from the biotite granite contains usually <0.1, exceptionally up to 2 wt.% Al_2O_3. Zircon from the more fractionated protolithionite stock granite contains between <0.1 and 3 wt.%, that from the zinnwaldite dyke granite between <0.1 and 5 wt.% Al_2O_3. In a P–Nb–Bi–Sc-rich zircon from the upper part of the zinnwaldite dyke granite, a maximum Al concentration of 5.5 wt.% Al_2O_3 (0.22 apfu Al) was determined (Table 3, anal. 18). Calcium usually displays a positive correlation with uranium. U-rich zircon from all types of rock contains up to 2–3 wt.% CaO, with the exception of one grain from the brecciated zinnwaldite dyke granite, which has incorporated 4.5 wt.% CaO (0.17 apfu Ca; Table 3, anal. 33). The distribution of iron is heterogeneous. Measured Fe abundances range mostly from 0.1 to 1.5 wt.% FeO, exceptionally approaching 3.59 wt.% FeO (0.103 apfu Fe; Table 3, anal. 2) in zircon from the biotite granite. The content of Th in all zircon types is low and usually less than <0.1 wt.% ThO_2. It exceptionally approaches 1–2 wt.%. The highest Th concentration (6.64 wt.% ThO_2, 0.055 apfu Th) was measured in an altered zircon from the upper part of the protolithionite stock granite (Table 3, anal. 6). The LREE abundances are mostly below their detection limits of the microprobe. The contents of Y and the HREE are variable at all scales and range between from below their detection limits to maximal 7.93 wt.% Y_2O_3 (0.145 apfu Y; Table 3, anal. 5). In zircon enriched in P, U, Al, Bi, Ca, Mn, Fe, and F, totals between 88 and 95 wt.% suggest the presence of significant quantities of water in the crystal structure.

Zircon from Podlesí contains normal to moderate Hf concentrations. The highest Hf concentration (9.1 wt.% HfO_2; equivalent to 8.5 mol% $HfSiO_4$) was determined in a zircon grain from the upper part of the protolithionite stock granite (Table 3, anal. 10). Noteworthy are the unexpectedly high and scattering Zr/Hf ratios in zircon from the extremely fractionated zinnwaldite dyke granite (mostly 5–25, up to 45), which are essentially higher than those commonly observed in zircon from fractionated pegmatites (2–5; Černý et al., 1985).

The vast majority of zircon from greisens (greisenised protolithionite stock granite and zinnwaldite dyke granite) has a composition close to endmember $ZrSiO_4$ and lacks evidence of alteration and metamictization (Table 3, anal. 15–16 and 35–36). These zircons are compositionally distinct from that in the granite parental to the greisens. However, there are also greisens, which contain zircons compositionally similar to those in their precursor, i.e., are rich in P, Al, U, and Bi (Table 3, anal. 37).

5. Discussion

It is impossible within the frame of this paper to thoroughly discuss all compositional features and the origin of all the various types of zircon from the Podlesí magmatic–hydrothermal system. This discussion will centre round the substitution mechanisms that gave rise to the extraordinary enrichment (and complimentary depletion) of a series of elements, which commonly occur as trace components in zircon. Furthermore, we will discuss the relative importance of magmatic versus postmagmatic (hydrothermal) processes in the origin of the chemically abnormal zircon from this locality.

5.1. Crystallization sequence of zircon

In the F-poor biotite granite, zircon crystallized as an early phase as recognized in common silicic magmas. Ongoing enrichment of F in the course of melt differentiation suppressed the nucleation of zircon from the more evolved Podlesí magmas, because fluorine increases the solubility of zircon in silicate melts (Keppler, 1993). In the final, highly fractionated and Zr-poor melts (20–40 ppm), crystallization of zircon started late, as result of the higher zircon solubility in F-rich melts.

5.2. Calculation of zircon formulae

The recalculation of the electron-microprobe analyses and creation of real formula of the studied zircons is not trivial. Ideally, the sum of all cations in octahedral (A-site) and tetrahedral (T-site) positions should equal 1 (A=T=1 for 4 oxygen atoms). If zircon contains substantial amount of interstitial cations (Hoskin et al., 2000; Finch and Hanchar, 2003), the sum of all cations per formula unit may be >2. On the other hand, substitution of $(OH)_4$ for SiO_4 decreases the sum of cations in the formula unit to <2. Because zircon contains both, structure-bound water (in the form of (H_4O_4) tetrahedrons) and adsorbed molecular water, calculation of the real amount of (H_4O_4)-tetrahedrons and thus, depletion of cations in tetrahedral positions, is impossible. To avoid speculative calculations, we assume in the Table 3 and in all diagrams that the sum of oxygen atoms totals 4. This simplification resulted in a slight surplus of the octahedrally coordinated cations (A=Zr+Hf+U+Th+Nb+Ta+Y+REE+Sc+Bi+Ca+Fe+Mn+Pb) relative to the tetrahedrally coordinated (T=Si+P+Al) cations (Fig. 6), and slight surplus of all cations (A+T>2) in circa 40% of all analysed grains (Fig. 7). The deficit on the T-site may well be explained by the substitution of $(OH)_4$ for SiO_4. The apparent surplus on the A-site is result of the presence of some elements (Ca, Al) in interstitial positions. The highest difference from the ideal formula (A+T>2.06) refers to zircon compositions distinguished by high contents of U+Ca (brabantite-type substitution). These zircons from the deeper part of the protolithionite stock granite probably contain important amounts of Ca^{2+} in interstitial position. Some Al-rich zircons display a sum of Si+P+Al>1, implying that a part of the analysed aluminium is also positioned interstitially.

5.3. Mineral inclusions in altered zircon – responsible for abnormal compositions?

The exotic composition of many of the zircon grains from this paper may question that the elements are part of the zircon structure, but instead are included in micro-inclusions not visible even in high-resolution BSE images. The following compositional and structural arguments could be provided arguing against such inclusions as important contaminants:

(a) In the situation of a mixture of pure zircon $(Zr,Hf)SiO_4$ with phosphates or silicates of Bi, Sc, Y, REE, U, Th, Al, Ca, Fe and Mn, the ratio (Zr+Hf)/Si should remain 1:1 (if the non-formula element are fixed in phosphates), or Si should slightly exceed Zr (if U is hosted in coffinite, Th in thorite, or Bi in emplektite, respectively). However, the majority of analysed
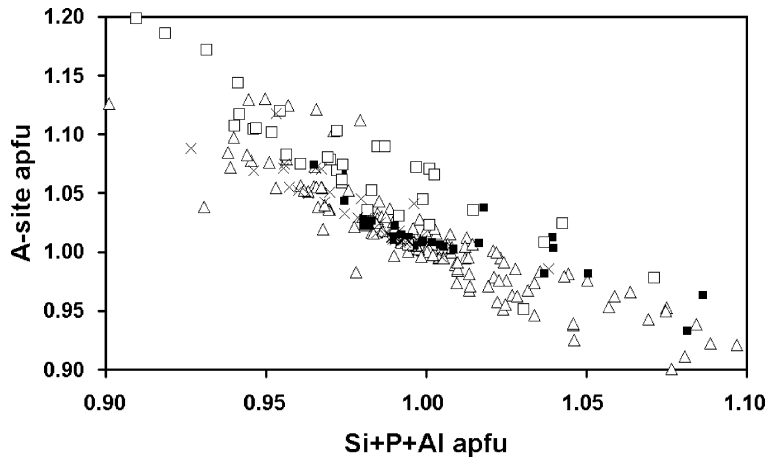
Fig. 6. Plot of T-site (Si+P+Al) versus A-site (all other cations) occupation in zircon. The excess on the A-site in some samples is related to the addition of all the Ca to the A-site elements, although a certain proportion of this cation, in reality, is located in interstitial position.

grains show a substantially higher cation deple-
tion in the T-site (Si-atoms) relative to the A-site
(Zr+Hf-atoms) (Fig. 8). Consequently, the major
part of phosphorus must have entered the T-site
in the zircon structure.
(b) Niobium and Ta may theoretically be present as
micro-inclusions of columbite. If so, one should
expect a correlation between (Nb+Ta) and
(Fe+Mn) and a ratio of (Nb+Ta)/(Fe+Mn) of
2:1 as in columbite. In our zircon analyses, Fe
and Mn systematically predominate over Nb (and
Ta) and do not correlate with them.
(c) Bismuth may be potentially fixed in Bi-phosphate
(ximengite) or Bi-silicate (emplektite). Neither
ximengite nor emplektite have been identified in
the studied samples as independent grains. There
is no plausible argument for their growth inside of
zircon.

(d) The potential hosts of (Y+HREE) and Sc—
xenotime and pretulite—are isostructural with
zircon. Thus, an isomorphic admixture of both
molecules in the zircon structure is likely to
occur, particularly because the mole percentages
of the xenotime and pretulite molecules in our
zircon samples is not particularly high.
(e) The presence of Al in tetrahedral coordination is a
common phenomenon in silicate minerals, where-
as the formation of Al-phosphates in altered zir-
con appears to be of much lesser probability.
(f) A few zircon grains from the deeper part of the
protolithionite stock granite display a Ca:U-ratio
of ~2:1. In most other zircons, Ca substantially
predominates over U, excluding unidentified
inclusions of monoclinic brabantite, which has a
Ca/(U+Th) ratio of 1:1, as the source for their
high contents of Ca (and U).
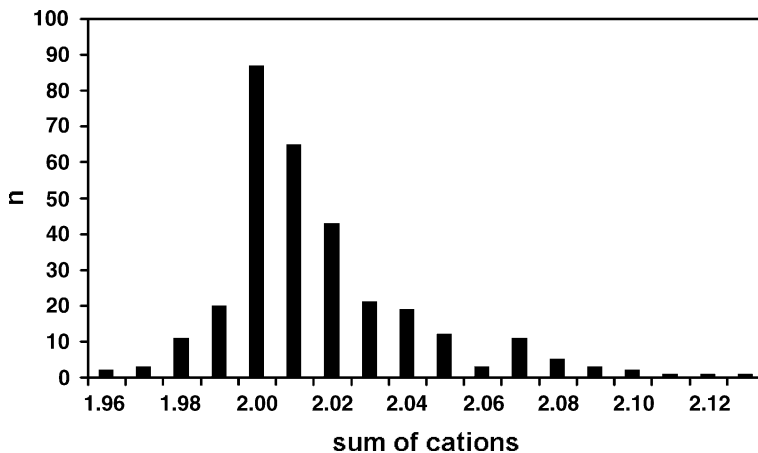
Fig. 7. Histogram showing the zircon cation sums calculated on the base of 4 oxygen atoms per formula unit.

133
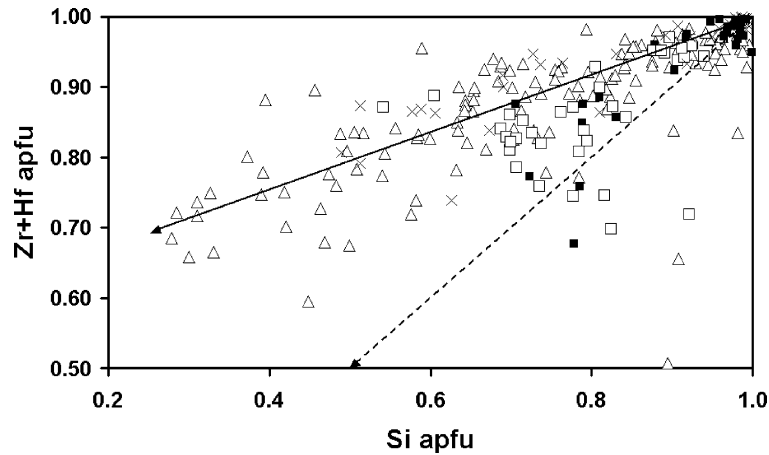
Fig. 8. Plot of Si versus (Zr+Hf) (in apfu). In case of a mixture of pure zircon (Zr,Hf)SiO$_4$ with phosphates or silicates of other analysed cations, the ratio (Zr+Hf)/Si remains 1:1 (dashed line, if the non-formula element are fixed in phosphates), or Si should slightly exceed Zr (if U is hosted in coffinite, Th in thorite, or Bi in emplektite, respectively). However, the majority of analysed grains show a significantly greater depletion of cations on the T-site relative to the A-site (full line), implying that the major part of the phosphorus must have entered the T-site in the zircon structure.

Altogether, no evidence exists for mineral inclusions being ultimately responsible for the significant derivation from endmember [(Zr, Hf)SiO$_4$] composition of many of the zircon grains from this study. However, we could not fully exclude the presence of nano-inclusions of some sort, the identification of which would require a spatial resolution higher than that of the electron microprobe.

5.4. Substitution of P in zircon

From the generally positive correlation between P and Al it can be concluded that a significant proportion of the P entered the tetrahedral Si-position according to the berlinite-type substitution $P^{5+}+Al^{3+} \Leftrightarrow 2\ Si^{4+}$. Operation of this substitution mechanism has already been suggested by Uher and Černý (1998) in their study of zircon from pegmatites in Slovakia. Interpretation of the analytical data from our study implies that a combination of the substitutions of berlinite-type and xenotime, $(REE+Y)^{3+}+P^{5+} \Leftrightarrow Zr^{4+}+Si^{4+}$, is most important in non-metamict, moderately P-enriched zircon. In metamict grains, P (in apfu) is usually substantially higher than the sum of Al+REE+Y implying that a major part of P is coupled with other trivalent and divalent elements in the A-site and in the interstices. In these grains, substitution reactions of the form $Sc^{3+}+P^{5+} \Leftrightarrow Zr^{4+}+Si^{4+}$ (pretulite), $Ca^{2+}+(U+Th)^{4+}+2P^{5+} \Leftrightarrow 2Zr^{4+}+2Si^{4+}$ (brabantite-type), and $Bi^{3+}+P^{5+} \Leftrightarrow Zr^{4+}+Si^{+}$ (ximengite-type) became increasingly more important (Fig. 6).

In a great number of analyses, the sum of P necessary to meet all the above-mentioned substitutions ac-

tually equals the amount of P analysed. However, some metamict grains, namely in the dyke granite, show a considerable deficiency, or a minor surplus, in P. One explanation for this depletion or increase may be a partial removal or accumulation of P in the metamict structure. Depletion of Si in the tetrahedral position often exceeded the sum of P and Al, i.e., $Si+P+Al<1$ 1 apfu, implying that further elements may have entered the Si-position. From an experimental study of synthetic, (REE+P)-doped zircon, Hanchar et al. (2001) suggested a small substitution of Zr into the (Si+P)-position, which was confirmed later qualitatively by single-crystal diffraction (Finch and Hanchar, 2003). Other substitutions include the entrance of H$_4$O$_4$ [or (OH)$_4$] for SiO$_4$. However, pentavalent elements Nb and Ta in A-site further complicate full understanding of the complex crystallography of the zircon from Podlesí.

In zircon from both types of greisenised granite, P correlates well with Sc at a ratio of 1:1 addressing the specific importance of the pretulite substitution ($Zr^{4+}+Si^{4+} \Leftrightarrow Sc^{3+}+P^{5+}$) for the incorporation of P and Sc in the crystal structure (Fig. 8).

5.5. Nature of the phosphorus enrichment

Although P constitutes an ubiquitous component in the majority of zircon from the evolved granites, we suggest that not all of the P is primary magmatic. The high peraluminosity (A/CNK=1.2–1.4), and the low calcium abundance (<0.2 wt.% CaO), in the evolved melt suppressed the crystallisation of apatite and facilitated the incorporation of P in the structure of late

crystallized silicate minerals. In Podlesí, the evolved granites contain albite with 1 wt.% P_2O_5, and K-feldspar with 1.5–2.0 wt.% P_2O_5 (Breiter et al., 2002; Breiter et al., 2005a). Topaz from the dyke granite contains up to 1 wt.% P_2O_5 (Breiter and Kronz, 2004). Considering that the berlinite substitution has triggered the incorporation of P in the late-magmatic silicates, we suggest that the portion of P in zircon coupled with Al may also be primary. This origin may as well hold for phosphorus associated with Y (xenotime substitution) and Sc (pretulite substitution). Enrichment of phosphorus coupled with enrichment of Ca (and other divalent elements) and the actinides (brabantite-type substitution) should be secondary, likely as result of metasomatism of metamict domains in zircon grains. The idea on metasomatic addition of P is supported by the circumstance that the most P-rich uranoan zircon from the biotite granite was observed in areas penetrated by thin dykes of highly fractionated, P-rich aplite. Infiltration of a P-rich fluid expelled from these aplites is suggested as the source of metasomatism of these zircon grains.

Zircon from the mica-rich and feldspar-poor fragments, and from the feldspar-rich and mica-poor matrix, in the brecciated zinnwaldite dyke granite differs significantly in composition (Fig. 5). Zircon from the fragments has a much higher U/P-ratio relative to that from the matrix. On the other hand, zircon from the matrix is much more enriched in Bi, Nb, and Ta. The reason for this compositional variation is poorly understood, but may be associated with differences in the contents of F, P, and water and in the hydrostatic pressure of the melts, from which the zircon precipitated (all these parameters were much higher at the time of crystallisation of the fragments; cf. Breiter et al., 2005a).

5.6. Metamictization, infiltration of P and Ca

The radioactive decay of uranium causes damage of the zircon structure, i.e., metamictization. Already 1 wt.% U resulted in full metamictization of the zircon structure after a period of 200 Ma (Meldrum et al., 1998). Previous studies yielded a maximum of 9.94% UO_2 in natural zircon (Huang, 2002). In Podlesí, almost all zircon grains from the stock and dyke granites have metamict, U-rich cores or patchy domains (commonly 0.5–2.0 wt.% UO_2, up to 14.75 wt.% UO_2 in the deeper protolithionite stock granite). Metamict areas in zircon are enriched in "non-formula" elements such as P, Ca, Fe, Al, Bi, and F. According to laboratory experiments (Geisler et al., 2002, 2003), low-temperature leaching

of metamict zircon should decrease its U content, but contemporaneously enrich the zircon in Ca, Fe, and Al. In Podlesí, there is a strong positive correlation between the abundances of U and those of the absorbed elements Ca, Fe, Al, and P in the individual zircon grains. This observation implies that the intensity of Ca, Al, Fe, and P metasomatism of the zircon is a function of the grade of metamictization, i.e., is related to its initial U content. On the other hand, these metasomatic reactions appear to stabilize the U in the zircon.

The lack of correlation between U and P, and between U and Ca, in the whole data set of zircon (compare Fig. 5) demonstrates that the percolation of P–Ca-bearing metasomatic fluids through the granite suite was highly irregular and, at many places, too low in quantity to effectively react with metamict zircon grains and alter their composition.

5.7. Enrichment of bismuth

In many zircon grains from Podlesí, incorporation of Bi was facilitated by the coupled substitution of P and Bi for Si and Zr. The natural Bi phosphate ximengite ($BiPO_4$) is trigonal (Shi, 1989), but its synthetic equivalent is monoclinic and isotype with monazite and huttonite (Strunz, 1970). Ximengite occurs as alteration product of bismuthinite in high-temperature quartz–cassiterite ores (Shi, 1989).

Bismuth belongs to those elements not routinely measured during electron-microprobe analysis of zircon. The only published record of Bi in zircon dates back to the 1950s, when Pavlenko et al. (1957) reported up to 5000 ppm Bi in zircon from an unnamed location in the former Soviet Union. In Podlesí, the Bi concentration in the zircon is not correlated with the Bi content of the host rock, which is high relative to that measured in common granitic rocks (see Table 1). The bulk-rock content of Bi is irregular but tends to increase with increasing degree of fractionation: mostly <2 ppm in biotite granite, 1–5 ppm in the protolithionite stock granite, and 5–10 ppm in the zinnwaldite dyke granite. However, individual samples from the Podlesí system contain up to hundreds of ppm Bi (zinnwaldite dyke granite up to 100 ppm, greisens up to 600 ppm).

Bi-rich zircon from the zinnwaldite dyke granite is associated with columbite enriched in Bi. Bismuthinite and bismuthite are frequent accessories in some samples through the whole magmatic–hydrothermal system in Podlesí. Other Bi minerals (native Bi, emplectite) are common constituent of many disseminated Sn–W mineralization in the Krušné Hory/Erzgebirge Mts. genetically associated with highly fractionated granites.

Therefore, it is reasonable to assume that the source of the Bi in Podlesí is the granite magma itself, and not Cretaceous hydrothermal fluids of the Ag–As–Bi–Co–Ni association, which has widespread expression also in the vicinity of Podlesí (e.g. Hösel et al., 1997). Whether Bi-rich zircon crystallized from late-stage magmas or high-T metasomatic fluids remains unresolved, but we tend to favour a hydrothermal origin of those zircon grains.

5.8. Enrichment of scandium

Natural pretulite ($ScPO_4$), which is isostructural with zircon, has been rarely reported from low-grade metamorphic rocks or sedimentary environments (Bernhard et al., 1998; Moëlo et al., 2002). In oolitic ironstones from Saint-Aubin-des-Châteaux in France, Moëlo et al. (2002) described phases intermediate between $ZrSiO_4$ and $ScPO_4$, which were interpreted by these authors as evidence for complete miscibility between the two end-members. An abundance of Zr similarly high than the maxima from this study was measured in a zircon from the Schugorsk bauxite deposit in Russia, (3.3 wt. Sc_2O_3; Mordberg et al., 2001). According to our knowledge, the highest content of Sc was determined in a zircon from the peraluminous Albuquerque granite in Spain related to U ore deposits (10.05 wt.% Sc_2O_3; Bea, 1996).

In the eastern Krušné Hory/Erzgebirge, enrichment of Sc was previously observed in ore minerals from Sn–W deposits (up to 1 wt.% Sc in wolframite from the Zinnwald and Krupka deposits; Breiter and Frýda, 1995). In Podlesí, wolframite and other Nb–Ta–W minerals are substantially Sc-poor (<0.05 wt.% Sc_2O_3, only individual spots up to 0.2 wt.% Sc_2O_3). Zircon is about one order of magnitude more enriched in Sc than the associated wolframite and columbite and appears to be the major host of Sc in Podlesí.

5.9. Enrichment of niobium and tantalum

Only a few zircons have been analyzed for Nb and Ta to date, and modern electron-microprobe analyses of these elements in zircon have been rarely performed. Wang et al. (2000) measured up to 0.12 wt.% Nb_2O_5 and 0.09 wt.% Ta_2O_5 in zircon from A-type granites in Laoshan, China. In a LA-ICPMS study, Belousova et al. (2002) determined a maximum of 3460 ppm Nb and 266 ppm Ta in a set of 588 analysed zircon grains collected from all igneous types of rock. According to our knowledge, 6.6 wt.% Nb_2O_5 measured in a zircon from pre-Variscan granites of the

Brno batholith, Czech Republic, represents the highest Nb concentration reported in the literature for this mineral (Leichmann et al., 1999). With 6.7 wt.% Nb_2O_5, zircon from Podlesi is slightly above this previous maximum. The contents of Ta are about one or two orders of magnitude lower than those of Nb and only rarely exceed the detection limit of the microprobe. A concentration of 1.36 wt.% Ta_2O_5 determined in one zircon grain from the brecciated dyke granite is exceptional. All Ta-enriched grains are also Nb-rich, but the small data set available precludes inferences on their overall correlation to be made. The whole-rock Nb/Ta ratios (in wt.% of oxides) decrease from about 4–5 in the biotite granites to about 2–3 in the late zinnwaldite dyke granite. The Nb/Ta ratio in their zircons is generally substantially higher, with 0.5–2.0 wt.% Nb_2O_5 usually coupled with <0.05 wt.% Ta_2O_5. The reason for this decoupling of geochemically similar elements in the course of their substitution into metamict zircon structure remains unresolved.

5.10. Enrichment of fluorine

According to our knowledge, only a few zircons have been analyzed previously for F. Uher and Černý (1998) reported up to 0.2 wt.% F in zircon from pegmatites in Slovakia. Uher et al. (1998) determined up to 0.2 wt.% F in zircon from a muscovite granite in southern Bohemia. Zircon from the Markersbach granite in the eastern Erzgebirge contain up to 0.46 wt.% F (Förster, 2000). Recently, Johan and Johan (2004) measured a maximum of 2.41 wt.% F in a zircon from the Cínovec/Zinnwald granite cupola. Contents between 2.0 and 3.5 wt.% F analyzed in zircon from the basal part of the Podlesí zinnwaldite dyke granite belong to the highest ever reported in zircon. Fluorine enrichment in zircon is in accordance with the high F content of the host granite (1–4 wt.%). An unexpected result of this study was the F poverty of the zircon from the greisens, although these rocks contain abundant F-bearing minerals: topaz, fluorapatite, and micas saturated in F. This may suggest that zircon in the greisens crystallized from a hydrothermal fluid that became impoverished in F as result of earlier precipitation of the F-rich minerals.

5.11. Fractionation of Hf

Linnen and Keppler (2002) determined a ratio of 2–5 for the partition coefficient of Zr and Hf (D_{Zr}/D_{Hf})

between zircon and a peraluminous granitic melt implying that the crystallization of zircon will decrease the Zr/Hf ratio of the melt. Indeed, in Podlesí, the whole-rock Zr/Hf atomic ratio decreases from 60–25 in the biotite granite, through 45–25 in the protolithionite stock granite, to 35–10 in the zinnwaldite dyke granite, i.e., by about 3 times. At the same time, the Zr/Hf atomic ratio in the zircon decreased from 100–50 in the biotite granite, through 60–30 in the protolithionite granite, to 40–15 in the zinnwaldite granite. The observation that the Zr/Hf ratio of the whole rock is partly lower than that of the respective zircon implies that a certain part of Hf is concentrated either in Hf-rich zircon rims to thin to be analysed by electron microprobe or in unanalysed small zircon grains. The large scatter of the zircon Zr/Hf ratio in all types of rock from Podlesí is expression of the different elemental substitutions that the zircon in Podlesí experienced. Evolution of zircon composition during fractionation of the Eibenstock granite massif in the western Erzgebirge, which belongs to the same, P–F-rich granite type as the Podlesí suite, suggests that for each granite type from Podlesí, the Zr/Hf ratios at the upper end of the ranges typify the normal magmatic evolution. Significant deviation from these values towards higher Zr/Hf ratios demonstrate that the substitution of one or more of the bizarre elements in the zircons under consideration occurred in expense of the hafnon relative to the zircon molecules, thereby increasing the Zr/Hf ratio of the zircon. The relative depletion of Hf, combined with a successive enrichment in Ca, Fe, Mn and Al was already mentioned from hydrous zircon from the Tanco pegmatite in Manitoba, Canada (Černý and Siivola, 1980).

The variation in the Hf concentration in zircon noticed in this study (0.85–9.1 wt.% HfO_2; 0.008–0.086 apfu Hf) significantly exceeds that recently reported for zircon from Podlesí by Kempe et al. (2004), 2–5 wt.%). However, it is in accordance with data for zircon from the P-rich Beauvoir granite, France (Wang et al., 1992) and fits within the range of Hf abundances in zircon from P-rich granites defined by Kempe et al. (2004); 2–9 wt.% of HfO_2). In equally high fractionated, but P-poor granites, zircon may incorporate up to 35 wt.% HfO_2 (Wang et al., 1996). Zircon from P-rich pegmatites is also able to incorporate significant amounts oh Hf in its structure: 13 wt.% HfO_2 in zircon from Chèdeville, France (Raimbault, 1998) or 15–18 wt.% HfO_2 in zircon from Tanco, Canada (Černý and Siivola, 1980). Consequently, P-enrichment in the granitic melt appears not a factor suppressing a more extensive Zr/Hf fractionation in zircon as observed at Podlesi. In perphosphorous granites, another, yet-unknown factor is in operation prohibiting a greater substitution of Hf in zircon relative to zircon from P-poor granites.

6. Summary and conclusions

Some zircon grains from the P–F-rich peraluminous granite system at Podlesí are extraordinarily depleted (Si, down to 0.30 apfu; Zr, down to 0.57 apfu) or enriched in several elements, which form trace components in ordinary zircon. Some of the elements enriched approach concentrations, which are novel or correspond to the highest reported to date. These elements include P (up to 20.2 wt.% P_2O_5; equivalent to 0.60 apfu), Bi (up to 9.0 wt.% Bi_2O_3; 0.086 apfu), Nb (up to 6.7 wt.% Nb_2O_5, 0.12 apfu), Sc (up to 3.45 wt.% Sc_2O_3; 0.10 apfu), U (up to 14.8 wt.% UO_2; 0.12 apfu) and F (up to 3.81 wt.% F; 0.42 apfu). The most important reactions responsible for the enrichment of some of these elements include the berlinite-type (P+Al), xenotime (Y/REE+P), brabantite-type (Ca+U), ximengite-type (Bi+P), and pretulite (Sc+P) substitutions. The formation of the abnormal zircon compositions can be attributed to a combination of two factors. One population of zircon crystallized late, from a P-, F- and water-rich melt high in Nb, Ta, Bi, and U, which has undergone a prolonged history of fractionation. These zircons then became further compositionally altered in result of the interaction with P- and F-rich postmagmatic fluids. The compositional signatures of zircon from strongly greisenized granites implies that zircon may completely dissolve and regrow during the interaction with greisenizing fluids of the sort that originated from the most fractionated residual melts at Podlesí.

This study demonstrates that low analytical totals frequently reported in the literature for electron-microprobe analyses of zircon from evolved granites and pegmatites may not only relate to the presence of water, but also to the presence of elements not sought for. To determine the entire spectrum of elements detectable by this method, careful WDS scans are recommended to conduct prior to microprobe analysis of "abnormal" zircon.

Acknowledgements

References

Bea, F., 1996. Residence of REE, Y, Th and U in granites and crustal protoliths; implications for the chemistry of crustal melts. J. Petrol. 37, 521–552.

Belousova, E.A., Griffin, W.L., OReilly, S.Y., Fisher, N.I., 2002. Igneous zircon: trace element composition as an indicator of source rock type. Contrib. Mineral. Petrol. 143, 602–622.

Bernhard, F., Walter, F., Ettinger, K., Taucher, J., Mereiter, K., 1998. Pretulite, ScPO4, a new scandium mineral from the Styrian and lower Austrian lazulite occurrences. Austria. Am. Mineral. 83, 625–630.

Breiter, K., Frýda, J., 1995. The Krupka tin deposit. In: Breiter, K., Seltmann, R. (Eds.), Ore Mineralizations of the Krušné Hory Mts. (Erzgebirge). Excursion guide Third Biennial SGA Meeting, Prague, August 28–31, 1995. Czech Geological Survey, Prague.

Breiter, K., Kronz, A., 2004. Phosphorus-rich topaz from fractionated granites (Podlesí, Czech Republic). Mineral. Petrol. 81, 235–247.

Breiter, K., Förster, H.-J., Seltmann, R., 1999. Variscan silicic magmatism and related tin–tungsten mineralization in the Erzgebirge–Slavkovský les metallogenic province. Mineral. Deposita 34, 505–521.

Breiter, K., Frýda, J., Leichmann, J., 2002. Phosphorus and rubidium in alkali feldspars: case studies and possible genetic interpretation. Bull. Czech Geol. Surv. 77, 93–104.

Breiter, K., Müller, A., Leichmann, J., Gabašová, A., 2005a. Textural and mineral evidence for evolution of fractionated granite magma: Podlesí granite stock, Czech Republic. Lithos 80, 323–345.

Breiter, K., Koller, F., Novák, M., Cempírek, J., 2005b. Phosphorus in garnet from leucocratic granites and granitic pegmatites; examples from the Bohemian Massif. Mineral Petrol. (in print).

Černý, P., Siivola, J., 1980. The Tanco pegmatite at Bernic lake, Manitoba: XII. Hafnian zircon. Can. Mineral. 18, 313–321.

Černý, P., Meintzer, R.E., Anderson, A.J., 1985. Extreme fractionation in rare-element granitic pegmatites: selected examples of data and mechanisms. Can. Mineral 23, 381–421.

Deer, W.A., Howie, R.A., Zussman, J., 1997. Rock-forming minerals. Orthosilicates, vol. 1A. Geological Society, London, pp. 418–442.

Eadington, P.J., Nashar, B., 1978. Evidence for the magmatic origin quartz–topaz rocks from the New England batholith, Australia. Contrib. Mineral. Petrol. 67, 433–438.

Finch, R.J., Hanchar, J.M., 2003. Structure and chemistry of zircon and zircon group minerals. In: Hanchar, J.M., Hoskin, P.W.O. (Ed.), Zircon, Reviews in Mineralogy and Geochemistry, vol. 53. Mineralogical Society of America, Geochemical Society. Washington DC, pp. 1–26.

Förster, H.-J., 1998. The chemical composition of REE–Y–Th–U-rich accessory minerals in peraluminous granites of the Erzgebirge–Fichtelgebirge region: Part I. The monazite–(Ce)–brabantite solid solution series. Am. Mineral. 83, 259–272.

Förster, H.-J., 2000. Synchysite–(Y)−synchysite–(Ce) solid solutions from Markersbach, Erzgebirge, Germany: REE and Th mobility

during high-*T* alteration of highly fractionated aluminous A-type granites. Mineral. Petrol. 72, 259–280.

Förster, H.-J., 2001. The radioactive accessory-mineral assemblage of the Podlesí granite–pegmatite system, western Krušné hory, Czech Republic: implication to intrusion age and magmatic/hydrothermal fluid–rock interaction. In: Breiter, K. (Ed.), International Workshop Phosphorus- and Fluorine-Rich Fractionated Granites, Podlesí. Abstracts and Excursion Guide. Czech Geological Survey, Praha, p. 22.

Förster, H.-J., 2006. Composition and origin of intermediate solid solutions in the system thorite–xenotime–zircon–coffinite. Lithos 88, 35–55. this volume.

Frýda, J., Breiter, K., 1995. Alkali feldspars as a main phosphorus reservoirs in rare-metal granites: three examples from the Bohemian Massif (Czech Republic). Terra Nova 7, 315–320.

Geisler, T., Pidgeon, R.T., van Bronswijk, W., Kurtz, R., 2002. Transport of uranium, thorium, and lead in metamict zircon under low-temperature hydrothermal conditions. Chem. Geol. 191, 141–154.

Geisler, T., Pidgeon, R.T., Kurtz, R., van Bronswijk, W., Schleicher, H., 2003. Experimental hydrothermal alteration of partially metamict zircon. Am. Mineral. 88, 1496–1513.

Hanchar, J.M., Finch, R.J., Hoskin, P.W.O., Watson, E.B., Cherniak, D.J., Mariano, A.N., 2001. Rare earth elements in synthetic zircons: Part 1. Synthesis, and rare earth element and phosphorus doping. Am. Mineral. 86, 667–680.

Hata, S., 1938. Xenotime and a variety of zircon from Iisaka. Scientific Papers of the Institute of Physical and Chemical Research 34, 619–622. (Tokyo).

Hösel, G., Tischendorf, G., Wasternack, J., Breiter, K., Kuschka, E., Pälchen, W., Rank, G., Štemprok, M., 1997. Erläuterungen zur Karte Mineralische Rohstoffe Erzgebirge-Vogtland/Krušné hory 1 : 100,000, Karte 2: Metalle, Fluorit/Baryt–Verbreitung und Auswirkung auf die Umwelt. Bergbau in Sachsen, 3. Sachsisches Landesamt für Umwelt und Geologie, Freiberg.

Hoskin, P.W.O., Schaltegger, U., 2003. The composition of zircon and igneous and metamorphic petrogenesis. In: Hanchar, J.M., Hoskin, P.W.O. (Eds.), Zircon, Reviews in Mineralogy and Geochemistry, vol. 53. Mineralogical Society of America, Washington DC, pp. 27–62.

Hoskin, P.W.P.O., Kinny, P.D., Wyborn, D., Chappell, B.W., 2000. Identifying accessory mineral saturation during differentiation in granitoid magmas: an integrated approach. J. Petrol. 41, 1365–1396.

Huang, X., 2002. variations in the mineralogy of the Yichun topaz–lepidolite granite, Jiangxi province, South China. Can. Mineral. 40, 1047–1068.

Huang, X.L., Wang, R.C., Chen, X.M., Liu, C.S., 2000. Study on phosphorus-rich zircon from Yashan topaz–lepidolite granite, Jiangxi province, South China. Acta Mineralogica Sinica 20, 22–27.

Johan, Z., Johan, V., 2004. Accessory minerals of the Cínovec (Zinnwald) granite cupola, Czech Republic: indicators of petrogenetic evolution. Mineral. Petrol 83 (36 pp.).

Kempe, U., Gruner, T., Renno, A.D., Wolf, D., Reno, M., 2004. Discussion on Wang et al. (2000). Chemistry of Hf-rich zircons from the Laoshan I- and A-type granites, Eastern China. Mineralogical Magazine, 64, 867–877. Min. Magazine 68, 669–675.

Keppler, H., 1993. Influence of fluorine on the enrichment of high field strength trace elements in granitic rocks. Contrib. Mineral. Petrol. 114, 479–488.

Kimura, K., Hironaka, Y., 1936. Chemical investigations of Japanese minerals containing rarer elements: XXIII. Yamagutilite, a phosphorus-bearing variety of zircon, found at Yamaguli Village, Nagano Prefecture. J. Chem. Soc. Japan 57, 1195–1199. (in Japanese).

Leichmann, J., Novák, M., Sulovský, P., 1999. Peraluminous wholerock geochemistry versus peralkaline mineralogy of highly fractionated, garnet-bearing granites from the Brno batholith. Eur. J. Mineral. 11 (1), 144. Beiheft.

Linnen, R.L., Keppler, H., 2002. Melt compositions control of Zr/Hf fractionation in magmatic processes. Geochim. Cosmochim. Acta 66, 3293–3301.

London, D., 1996. Granitic pegmatites. Trans. Royal Soc., Edinburgh. Earth Sci. 87, 305–319.

Meldrum, A., Boatner, L.A., Weber, W.J., Ewing, R.C., 1998. Radiation damage in zircon and monazite. Geochim. Cosmochim. Acta 62, 2509–2520.

Moëlo, Y., Lulzac, Y., Rouer, O., Paldaveau, P., Gloaguen, E., Léone, P., 2002. Scandium mineralogy: pretulite with scandian zircon and xenotime-(Y) within an apatite-rich oolitic ironstone from Saint-Aubin-des-Châteaux, Armorican Massif, France. Can. Mineral. 40, 1657–1673.

Mordberg, L.E., Stanley, C.J., Germann, K., 2001. Mineralogy and geochemistry of trace elements in bauxites: the Devonian Schugorsk deposit, Russia. Mineral. Mag. 65, 81–101.

Pavlenko, A.S., Vainshtein, E.E., Shevaleevskii, I.D., 1957. On the Hf–Zr ratio in zircons of igneous and metasomatic rocks. Geochemistry 1957, 411–430.

Pouchou, J.L., Pichoir, F., 1985. "PAP" (φ–ρ–Z) procedure for improved quantitative microanalysis. In: Armstrong, J. (Ed.), Microbeam Analysis. San Francisco Press, pp. 104–106.

Raimbault, L., 1998. Composition of complex lepidolite-type granitic pegmatites and of constituent columbite–tantalite, Chedeville, Massif Central, France. Canad. Mineral. 36, 563–583.

Raimbault, L., Burnol, L., 1998. The Richemont rhyolite dyke, Massif Central, France: a subvolcanic equivalent of rare-metal granites. Can. Mineral. 36, 265–282.

Shannon, J.R., Walker, B.M., Carten, R.B., Geraghty, E.P., 1982. Unidirectional solidification textures and their significance in determining relative ages of intrusions at the Henderson Mine, Colorado. Geology 10, 293–297.

Shi, J., 1989. A new mineral; ximengite. Chinese J. Geochem. 8, 385–391.

Speer, J.A., 1982. Zircon. In: Ribbe, P.H. (Ed.), Reviews in Mineralogy, second ed. Orthosilicates, vol. 5. Mineralogical Society of America, pp. 67–112.

Strunz, H., 1970. Mineralogische Tabellen: 5. Auflage. AV Geest and Portig K.-G., Leipzig.

Uher, P., Černý, P., 1998. Zircon in Hercynian granitic pegmatites of the Western Carpathians, Slovakia. Geol. Carpathica 49, 261–270.

Uher, P., Breiter, K., Klečka, M., Pivec, E., 1998. Zircon in highly evolved Hercynian Homolka granite, Moldanubian zone, Czech Republic: indicator of magma source and petrogenesis. Geol. Carpathica 49, 151–160.

Wang, R.C., Fontan, F., Xu, S.J., Monchoux, P., 1992. Hafnian zircon from the apical part of the Suzhou granite, China. Can. Mineral. 30, 763–1010.

Wang, R.C., Fontan, F., Xu, S.J., Chen, X.M., Monchoux, P., 1996. Minéraux disséminés comme indicateurs du caractère pegmatitique du granite de Beauvoir, massif dEchassières, Allier, France. Can. Mineral. 34, 1001–1770.

Wang, R.C., Zhao, G.T., Lu, J.J., Chen, X.M., Xu, S.J., Wang, D.Z., 2000. Chemistry of Hf-rich zircons from the Laoshan I- and A-type granites, Eastern China. Mineral. Mag. 64, 867–877.

Xiong, X.L., Zhao, Z.H., Zhu, J.C., Rao, B., 1999. Phase relations in albite granite–H_2O–HF system and their petrogenetic application. Geochem. J. 33, 199–214.